

# SWAG: Long-term Surgical Workflow Prediction with Generative-based Anticipation

Maxence Boels\*, Yang Liu, Prokar Dasgupta,  
Alejandro Granados, Sebastien Ourselin

Surgical and Interventional Engineering, King’s College London.

\*Corresponding author(s). E-mail(s): [maxence.boels@kcl.ac.uk](mailto:maxence.boels@kcl.ac.uk);

## Abstract

**Purpose** While existing recognition approaches excel at identifying current surgical phases, they provide limited foresight into future procedural steps, restricting their intraoperative utility. Similarly, current anticipation methods are constrained to predicting short-term events or singular occurrences, neglecting the dynamic and sequential nature of surgical workflows. To address these limitations, we propose SWAG (Surgical Workflow Anticipative Generator), a unified framework for phase recognition and long-term anticipation of surgical workflows.

**Methods** SWAG employs two generative decoding methods—single-pass (SP) and auto-regressive (AR)—to predict sequences of future surgical phases. A novel prior knowledge embedding mechanism enhances the accuracy of anticipatory predictions. The framework addresses future phase classification and remaining time regression tasks. Additionally, a regression-to-classification (R2C) method is introduced to map continuous predictions to discrete temporal segments. SWAG’s performance was evaluated on the Cholec80 and AutoLaparo21 datasets.

**Results** The single-pass classification model with prior knowledge embeddings (SWAG-SP\*) achieved 53.5% accuracy in 15-minute anticipation on AutoLaparo21, while the R2C model reached 60.8% accuracy on Cholec80. SWAG’s single-pass regression approach outperformed existing methods for remaining time prediction, achieving weighted mean absolute errors of 0.32 and 0.48 minutes for 2- and 3-minute horizons, respectively.

**Conclusion** SWAG demonstrates versatility across classification and regression tasks, offering robust tools for real-time surgical workflow anticipation. By unifying recognition and anticipatory capabilities, SWAG provides actionable predictions to enhance intraoperative decision-making. The project webpage is available at <https://maxboels.github.io/swag>.

**Keywords:** Surgical Workflow Anticipation, Surgical Phase Recognition, Generative Models, Cholec80, AutoLaparo21

# 1 Introduction

**S**URGICAL WORKFLOW ANTICIPATION has the potential to enhance operating room efficiency and patient safety by predicting future surgical phases during procedures. Anticipating surgical steps allows for better preparation, reduces cognitive load on surgeons, and improves coordination among surgical teams [1, 2]. While preoperative planning provides an initial framework, it often falls short in addressing the dynamic environment and decision-making required during surgery.

Current approaches predominantly focus on surgical phase recognition, identifying the present phase, step, or action [3–5]. These methods are valuable for postoperative analysis but offer limited assistance in real-time intraoperative decision-making. They lack the ability to anticipate future events, which is crucial for dynamic planning and improving surgical outcomes.

Some studies have explored surgical workflow anticipation by predicting the remaining time until the end of surgery [6–11], next phases, and instruments occurrence [12, 13]. However, these methods are limited by the need to predict a single event per class, disregarding scenarios with multiple future occurrences within a fixed time horizon.

Generative models, such as GPT models [14], address this challenge by generating sequences of tokens of arbitrary length and class repetition. In surgical workflow anticipation, auto-regressive [14] and single-pass decoding models [15] demonstrate the potential to predict continuous, coherent sequences of surgical actions. Unlike conventional discriminative and regressive approaches, generative models output multiple future tokens to directly construct the future sequence, continuing the temporal structure between observed input and generated outputs. Our work leverages both auto-regressive and single-pass approaches, allowing for predictions of arbitrary sequence lengths and frequencies that retain continuity and better mirror the evolving nature of surgical workflows.

In this work, we present SWAG (Surgical Workflow Anticipative Generator), a generative model designed to unify phase recognition and future anticipation of surgical workflows. Our main contributions are as follows:

1. We introduce SWAG, a generative model that integrates surgical phase recognition and anticipation for long-term and dense future prediction of workflows.
2. We provide an extensive comparison of two generative decoding methods—single-pass (SP) and auto-regressive (AR)—alongside two tasks—classification and regression—to generate sequences of future surgical events.
3. We propose a novel prior knowledge embedding mechanism using class-conditional probabilities to initialise generated future tokens, enhancing anticipation accuracy.
4. We conduct a comprehensive evaluation on the Cholec80 and AutoLaparo21 datasets, demonstrating SWAG’s performances on different surgical workflows.

## 2 Related Work

**Surgical Phase Recognition.** Early research on surgical phase recognition relied on probabilistic graphical models with instrument usage [16]. Later, convolutional neural networks were used to learn spatial representations from surgical video frames, while temporal relations among video frames were captured with recurrent neural networks [17]. Temporal convolutional networks were later able to increase the receptive field [3]. Masked self-attention in Transformers enabled learning causal dependencies from sequential data with high parallelism [18]. This self-attention mechanism was later used in the Vision Transformer (ViT) [19] to capture global context regardless of the spatial distance between pixels. Recent works have successfully used Transformers to capture critical information between frames using short attention windows like in Trans-SVNet [20] and LoViT [4], whereas SKiT [5] proposed an efficient long-term compression approach achieving state-of-the-art performance on online surgical phase recognition. Although these approaches offer substantial advancements for postoperative video analysis, we focus on intraoperative decision-making by adding anticipative capabilities to the recognition system. This anticipatory approach could enhance real-time decision support by forecasting upcoming surgical phases, enabling smoother, more responsive guidance during procedures.

**Surgical Workflow Anticipation.** Most anticipation approaches in surgery have explored surgical workflow anticipation by predicting the remaining time until the end of surgery [6–11], next instruments [12] or next phases occurrence [13]. A Bayesian model in [12] was proposed to anticipate tool usage which was then used as a baseline in [13] for surgical phase anticipation. [13] introduced IIA-Net, leveraging instrument interaction for next-phase occurrence regression. Although IIA-Net requires pre-trained models for tool detection and segmentation, we compare our method to this approach and their implementation of Bayesian [12]. Both methods were formulated as a regression problem, for surgical phase anticipation. Other methods were proposed for gesture anticipation as low-level motion planning [21], instrument trajectory prediction [22, 23], and a generative adversarial network was used in [24] to predict future surgical phases within the next 15 seconds. Action triplets were predicted over 4 seconds in [25], while [26] proposes a graph network with bounding boxes as inputs to predict the occurrence of instruments or phases within 2-, 3-, and 5-minutes horizons. Most methods focus on the next occurrence regression, failing to provide a comprehensive view of the entire surgical workflow, leaving a blind spot for events beyond the first predicted occurrence. Unlike previous works, SWAG uses a generative approach for future sequence classification. Our approach addresses some gaps and limitations by predicting sequences of arbitrary length and frequency, and unifying recognition and anticipation tasks.

## 3 Methods

In this section, we present our proposed method for jointly addressing recognition and anticipation tasks in surgical workflow prediction. Our model, SWAG, is designed to

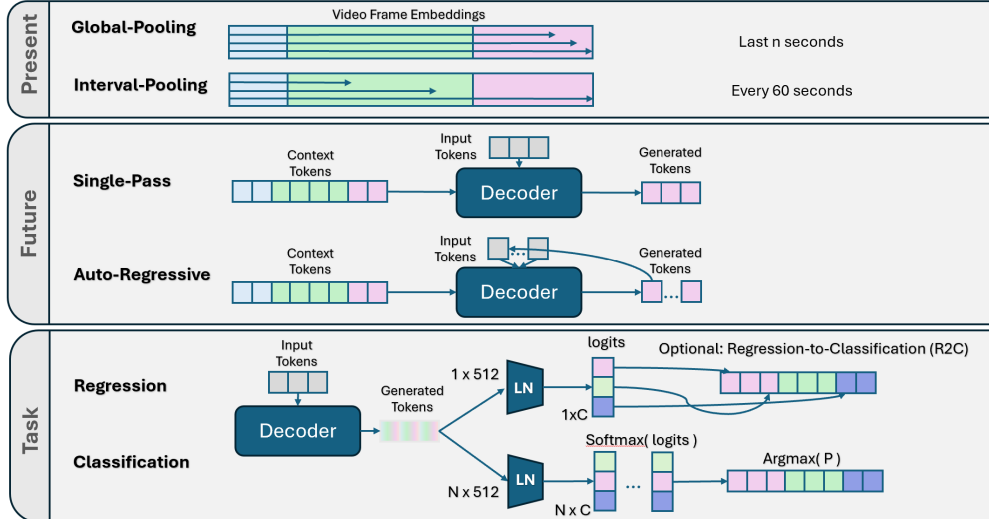


**Fig. 1:** Comparison of temporal pooling methods (top) for aggregating past to present contextual information, generative—single-pass and auto-regressive—methods (middle), and network layers for the regression and classification tasks (bottom).

predict current phases while anticipating the occurrence of future phases over long-time horizons. The SWAG architecture consists of multiple modules, each described in detail below, and is evaluated through a range of experiments.

### 3.1 Task Formulation

Our primary task is to predict future surgical phases, either as classification or regression, based on observed video frames over a long-term horizon of up to  $N$  minutes. Based on our ablation studies and previous works, we predict future phases every 60 seconds and evaluate over short- to long-term horizons. We can express the classification task as:

$$f_{\theta} : x_{\leq t} \mapsto (y_{t+(1*60)}, y_{t+(2*60)}, \dots, y_{t+(N*60)}) \quad (1)$$

where  $x_{\leq t}$  denotes all video frames up to and including the current time  $t$ ,  $y_{t+n*60}$  is the predicted surgical phase label  $n$  minutes after time  $t$ .

For the regression task, our goal is to predict the remaining time until the next occurrence of each surgical phase within a future horizon of  $h$  minutes. For each phase, the model outputs a predicted remaining time in minutes. These predictions are constrained within the range  $[0, h]$ : a value of 0 means the phase is currently occurring, while a value of  $h$  indicates that the phase will not occur within the upcoming  $h$  minutes.

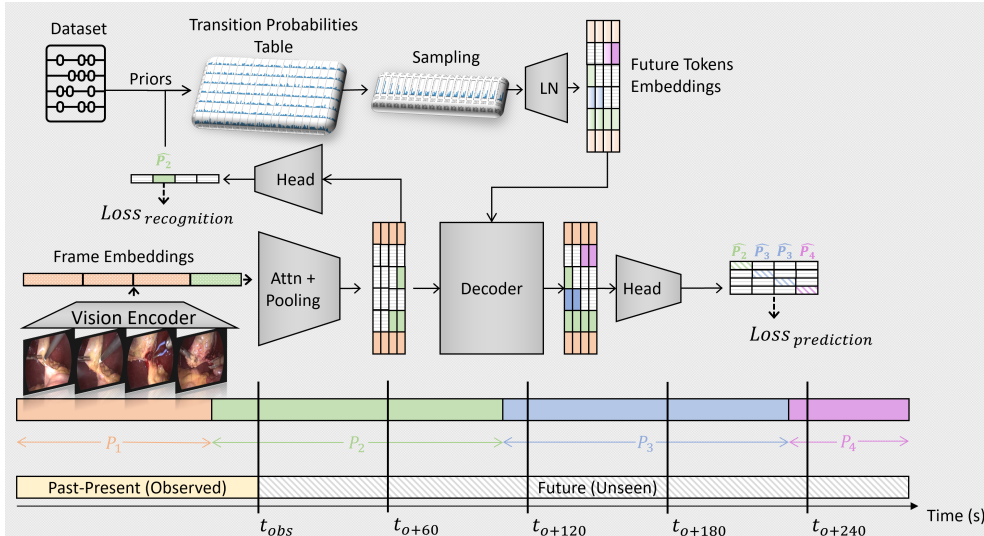


**Fig. 2:** Overview of the SWAG model architecture. The model employs single-pass future token prediction with prior probability embeddings sampled from the current recognized class and anticipated temporal positions.

### 3.2 SWAG Model Architecture

Our proposed model, illustrated in Figure 2, comprises a vision encoder, a temporal aggregation module based on self-attention, compression and pooling mechanisms, and a future prediction module that can operate with either a single-pass (SP) or an auto-regressive (AR) decoder. While our model uses classification for the recognition task, it can use either classification or regression for anticipation. This architecture also includes a novel token embedding initialization strategy based on the recognised class and the temporal position of the decoded target token.

**Vision Encoder.** Similar to LoViT [4], we fine-tune a pre-trained ViT [19] to learn short spatiotemporal representations  $f_t$  from surgical video frames.

**Temporal Self-Attention.** To recognise the observed frames at time  $t$ , we use a clip  $c_t = \{f_{t-l}, \dots, f_t\}$  of latent representations as our model input, where  $f_t$  is the embedding at the current time and  $l$  is the length of the input clip. We then use a short sliding window of length  $w$  to perform self-attention on the long input clip  $c_t$  with no overlap and get an output sequence of the same length,  $E_t = \{e_{t-l}, \dots, e_t\}$ .

**Compression and Pooling.** To address the need for long-term dependencies, we follow SKiT [5] and aggregate the full clip sequence of short-term spatiotemporal features  $E_t = \{e_{t-l}, \dots, e_t\}$  with temporal max-pooling and compress their features representation into a lower dimensional latent space  $d = 64$  as  $K_t = \{k_{t-w}, \dots, k_t\}$  to capture the most relevant information, resulting in  $w$  vectors. We illustrate our model’s temporal aggregation and generative method in Figure 1. The auto-regressive approach uses a causal decoder with a 60-second anticipation time for input frames, ensuring temporal consistency across the input context and the generated output

tokens. Our interval-pooling technique compresses 60 frame embeddings into a single token, each representing 1 minute of video content. We evaluate four combinations of these approaches and methods in our ablation studies, enabling a comprehensive assessment of their impact on model performance.

**Future Decoder.** Our proposed Single-Pass (SP) and Auto-Regressive (AR) approaches use a Transformer-based decoder to predict future tokens  $S$ , which are then used to estimate the surgical phase probabilities for each future time step. We project the compressed pooled features,  $K_t = \{k_{t-w}, \dots, k_t\}$ , to a higher dimension  $d = 512$  with a linear layer and pass it to our decoder as our input context. Our future token input queries are embedded with prior future class probabilities. Our two approaches can be described as follows:

1) *Single-Pass (SP)*: The decoder receives and generates all  $N$  tokens simultaneously, representing every 60 seconds over  $N$  minutes,  $S = \{s_1, s_2, \dots, s_N\}$ . This approach processes the input context  $K_t$  once to generate all future tokens, allowing for efficient parallel computing and reducing inference time.

2) *Auto-Regressive (AR)*: The decoder generates future tokens sequentially, one at a time. Starting with  $K_t$ , it predicts the next token  $s_1$ . For each subsequent step  $i$ , it uses  $K_t$  and all previous tokens  $\{s_1, \dots, s_{i-1}\}$  to produce  $s_i$ , until all  $N$  tokens are generated.

**Present Classifier.** Similar to SKiT, we first fuse the key-pooled features with the short-term spatiotemporal features using a skip connection. The resulting fused feature vector is then passed through a classification layer to predict class probabilities for  $\hat{p}_{t-w}, \dots, \hat{p}_t$ . The final prediction  $\hat{y}_t$  for frame  $x_t$ , takes the last frame’s class probabilities,  $\hat{p}_t$ , which is trained using a cross-entropy loss function.

**Future Prediction.** We use a classification layer as our primary model architecture to assign future tokens to classes. Alternatively, we use a linear layer for the regression task and predict the remaining time until the next phases and Remaining Surgery Duration (RSD). Finally, we propose a regression-to-classification (R2C) method which maps the predicted logits values for each class to classify future frames.

### 3.3 Prior Knowledge Embedding

To enhance the model’s predictive capabilities, we incorporate prior knowledge through class conditional probabilities. Specifically, we compute the probabilities of transitioning from the current recognised class to future classes at different anticipation times. Let  $C_t$  denote the class at time  $t$ , and  $P(C_{t+\tau} = j \mid C_t = i)$  represent the probability of transitioning to class  $j$  at time  $t + \tau$  given the current class  $i$ . We construct a probability tensor  $P$  where each entry  $P_{i,j,\tau}$  corresponds to this conditional probability for all classes  $i, j$  and anticipation times  $\tau$ . During training, we use these probabilities to initialize the embeddings of future tokens. Specifically, for each future token at time  $t + \tau$ , we initialize its embedding using the probability distribution  $P_{i,:,\tau}$ , where  $i$  is the current recognised class.

### 3.4 Experimental Setup

**Datasets.** We evaluate our work on two publicly available surgical phase recognition datasets: *Cholec80* (C80) [27] and *AutoLaparo21* (AL21) [28]. In C80, for the classification task, we use the 40-40 split for training and evaluation as in [4, 20], whereas, for the regression task, we use the 60-20 split following [12, 13]. For C80 and AL21, we train on the seven surgical phases, including an additional end-of-surgery (EOS) class, while disregarding tool annotations. In AL21, we follow the same 14/7 split for training and testing as in [4]. Both datasets were sampled at 1 frame per second (fps) following previous works [4, 20].

**Anticipation Time.** We assess our method over a range of prediction horizons to capture both short-term (2, 3, and 5 minutes) and long-term (15, 30, 60, and 90 minutes) events. Given that C80 procedures have an average duration of 38 minutes and AL21 procedures average 66 minutes, extending phase predictions up to 90 minutes captures each procedure’s full workflow. This range enables us to simultaneously predict immediate transitions and estimate the remaining surgery duration.

**Classification Task.** Since long-term future phase classification has not been studied in previous work, direct comparisons to other surgical workflow anticipation methods are not possible. Therefore, we assess our generative approaches against two baseline methods: a simple continuation model (Naive1) and a probabilistic prediction model (Naive2). **Naive1** ( $R*N$ ) baseline extends the current recognized class over the future prediction dimension for  $N$  minutes. While effective for short-term predictions, its performance naturally degrades over time with new class transitions. **Naive2** ( $R + P_{i,j,\tau}$ ) baseline uses the recognised current class and the predicted future token index to sample from a probability distribution  $P_{i,j,\tau}$ . Naive2 is a strong baseline due to the robust priors given the correct observed phase and future anticipation time.

**Regression Task.** We include a secondary evaluation to compare our method to previous works. Specifically, we benchmark against Bayesian [12] and II-Net [13], both of which predict the remaining time until the next phase occurrence. While II-Net incorporates instrument presence labels for supervision, we maintain consistency by focusing solely on video frame data. We did not include results from the TransSVNet [29] method as their evaluation was limited to a single horizon (5 minutes). We extend the phase anticipation regression task to long horizons to include the remaining surgery duration (RSD) evaluation following previous works [7, 9, 10].

### 3.5 Evaluation Metrics

We use a combination of classification and regression metrics to evaluate our methodology. These metrics are calculated for each anticipation time, allowing us to analyse the model’s performance through time. We use the frame-based accuracy to measure the proportion of correctly classified frames among all predictions. Finally, we use the Mean Absolute Error (MAE) to evaluate the model’s performance on the regression task, specifically for predicting the remaining time until the next phase occurrence. This metric quantifies the average absolute prediction errors in minutes. We use the  $wMAE$ ,  $inMAE$ , and  $outMAE$  for *weighting* samples *outside* and *inside* the temporal horizon as proposed in [12, 13], respectively.

## 4 Results

We present our experimental results on both classification and regression tasks, comparing our models to naïve baselines and state-of-the-art methods.

### 4.1 Surgical Phase Anticipation with Sequence Classification

Table 1 summarises the classification results for phase anticipation at 2, 3, 5, and 15-minute horizons across Cholec80 and AutoLaparo21 datasets. On Cholec80, SWAG-R2C achieves superior performance in mid- to long-term horizons, with an anticipation accuracy of 69.2% at 5 minutes and 60.8% at 15 minutes, closely followed by SWAG-AR at shorter time horizons. The Naive1 baseline performs well for short-term anticipation, achieving the highest 2-minute accuracy on both Cholec80 (78.6%) and AutoLaparo21 (71.6%). This success arises from its simple approach of extending the current phase over the prediction window, which leverages short-term phase stability. However, as anticipation horizons increase, Naive1’s accuracy declines significantly (43.0% on Cholec80, 44.9% on AutoLaparo21 at 15 minutes) due to an inability to handle frequent phase transitions.

**Table 1: Surgical Phase Anticipation with Classification.**  $Acc_{\tau_i}$ : phase anticipation from 0 to  $t$  minutes ahead.

Methods	Cholec80 (40/40)				AutoLaparo21 (14/7)			
	$Acc_{\tau_2}$	$Acc_{\tau_3}$	$Acc_{\tau_5}$	$Acc_{\tau_{15}}$	$Acc_{\tau_2}$	$Acc_{\tau_3}$	$Acc_{\tau_5}$	$Acc_{\tau_{15}}$
Naive1	<b>78.6</b>	73.9	<u>66.1</u>	43.0	<b>71.6</b>	<b>68.7</b>	<b>63.7</b>	44.9
Naive2	75.3	70.9	64.2	52.6	67.5	63.7	58.1	46.8
SWAG-AR	78.1	<b>74.6</b>	<b>69.2</b>	53.4	<u>70.2</u>	<u>67.6</u>	<u>62.8</u>	45.9
SWAG-SP	57.9	54.4	50.8	49.9	57.4	54.8	51.2	51.6
SWAG-SP*	71.0	67.3	62.5	<u>54.3</u>	66.3	63.8	60.1	<b>53.5</b>
SWAG-R2C	75.7	73.3	<b>69.2</b>	<b>60.8</b>	60.5	60.3	58.2	<u>52.2</u>

**Note:** The light blue cells in bold and underlined values are the best and second-best results, respectively. \* indicates the presence of our prior knowledge token embedding initialization method.

Overall, SWAG-SP\* demonstrates the highest performance on AutoLaparo21 for long-term horizons, achieving an anticipation accuracy of 53.5% at 15 minutes, which outperforms all our methods, including the auto-regressive model. SWAG-SP\* shows a marked improvement in accuracy over its SP counterpart on all anticipation times and datasets. The performance of naive and proposed models is depicted at minute intervals along with the recognition task at time 0 in Figure 3. SWAG-SP\* and SWAG-R2C achieve higher accuracy across 18 minutes, particularly excelling at longer anticipations.

### 4.2 Surgical Phase Anticipation with Remaining Time Regression

We compare the performance of our proposed single-pass model to previous work when trained to anticipate the remaining time until the next phase occurrence (see Table 2). For 2-minute and 3-minute horizons, SWAG-SP achieves the best inMAE



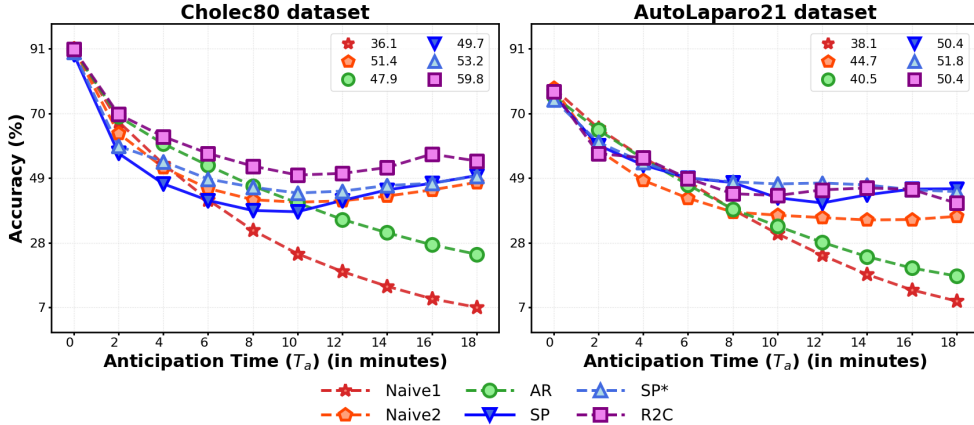


**Fig. 3:** Model performance (accuracy) of surgical phase recognition and anticipation on Cholec80 and AutoLaparo21 up to 18 minutes, with mean values over 18 minutes.

scores (0.54 and 0.77 minutes for 2 and 3 minutes), outperforming Bayesian [12] and IIA-Net [13]. At the 5-minute horizon, SWAG-SP ranks second with its wMAE score, showing strong adaptability for mid-range anticipations. Unlike IIA-Net [13], which uses additional inputs like instrument bounding boxes and segmentation maps, our approach relies solely on raw video frame inputs.

**Table 2: Remaining time to Phases at 2, 3, and 5 minutes before occurrence.** MAEs (in minutes) for *inside* and *outside* the anticipation window, and *weighted* mean.

Methods	Cholec80 (60-20)								
	<i>wMAE</i> [↓]			<i>inMAE</i> [↓]			<i>outMAE</i> [↓]		
	2 min	3 min	5 min	2 min	3 min	5 min	2 min	3 min	5 min
Bayesian[12]	0.39	0.59	0.85	0.63	0.86	<u>1.17</u>	0.15	0.32	0.52
IIA-Net [13]	<u>0.36</u>	0.49	<b>0.68</b>	0.62	0.81	<b>1.08</b>	0.10	0.18	0.28
SWAG-SP	<b>0.32</b>	<b>0.48</b>	<u>0.80</u>	<b>0.54</b>	<b>0.77</b>	1.26	<b>0.09</b>	<b>0.17</b>	0.34

**Note:** The light blue cells in bold and underlined values are the best and second-best results, respectively.

In the next experiment, we provide quantitative results over long-term horizons of up to 60 minutes for both the Cholec80 and AutoLaparo21 datasets, evaluating the model’s performance in future phase occurrence and Remaining Surgery Duration (RSD) regression (see Fig. 4). We assess SWAG-SP’s long-term phase anticipation performance per phase, including the end-of-surgery (EOS) class, on both datasets.

On the Cholec80 dataset, we observe an increasing error from approximately 2 to 8 minutes for mid- to late-stage surgical phases, specifically classes 4, 5, 6, and EOS. In contrast, anticipation errors for phases 2 and 3 remain stable over time, averaging around 5.5 minutes. The model exhibits an error below 1 minute for phase 1, likely

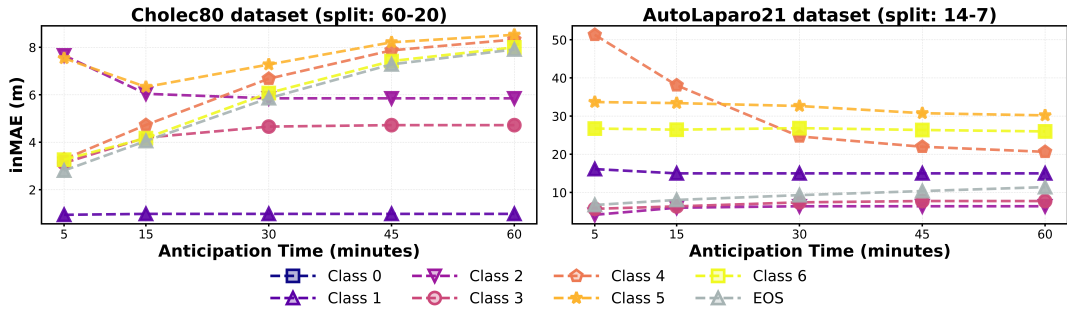


Fig. 4: Inside MAE Per-Class insideMAE on Cholec80 and AutoLaparo21.

because phase 1 occurs at the very beginning of the surgery, leading the model to predict low values that are often accurate.

For the AutoLaparo21 dataset, the task is more challenging, especially for mid-to late-phase stages, though the EOS class is less impacted. Errors are less correlated with time, reflecting the intrinsic uncertainty of phase variability. Classes 4, 5, and 6, in particular, are inconsistently present and often exhibit abrupt transitions, making prediction difficult. Over long horizons, the model takes a conservative approach by predicting mid-range values. However, as it nears the 5-minute horizon, it attempts to predict lower, more specific values, which can lead to substantial errors if the phase is absent or has sudden transitions.

As shown in Fig. 4, our model maintains stable performance on both Cholec80 and AutoLaparo21 for Remaining Surgery Duration estimation (grey triangles), with errors averaging below 10 minutes over a 60-minute anticipation horizon.

In Table 3, we compare our method with previous approaches. Using 4-fold cross-validation, our model ranks second on MAE-5 and MAE-ALL, outperforming multiple methods specifically designed for this task. These results underscore our model’s versatility across several benchmarks.

**Table 3: Remaining Surgery Duration (RSD) estimation on Cholec80.** Those results were reported in BD-Net.

Methods	MAE-5 (min)	MAE-30 (min)	MAE-ALL (min)
TimeLSTM [6]	3.00 ± 1.87	5.30 ± 1.86	8.27 ± 6.25
RSDNet [7]	8.36 ± 3.71	6.83 ± 2.57	10.01 ± 6.54
CataNet [9]	2.47 ± 2.62	5.53 ± 2.75	8.27 ± 6.81
BD-Net [10]*	<b>1.97 ± 1.54</b>	<b>4.84 ± 2.31</b>	<b>7.75 ± 6.43</b>
SWAG-SP (ours)	2.24 ± 2.32	6.48 ± 3.85	8.18 ± 5.33

**Note:** \* This method randomly created 4-splits for validation, whereas we used consecutive 60/20 splits for training and testing, respectively.

## 5 Discussion

In this work, we introduce SWAG, a unified approach for surgical phase recognition and anticipation, employing two generative models—single-pass and auto-regressive

decoding methods. The SWAG framework supports both classification and regression-based predictions, each bringing unique advantages to surgical workflow anticipation.

Our study centres on generative models for the sequential classification of future surgical phases, proposing two SWAG variants: single-pass (SP) and auto-regressive (AR) decoding. We demonstrate how prior knowledge can be used to initialise future tokens in single-pass decoding (SP\*), resulting in improved performance. The remaining time prediction from the single-pass approach can also be converted into class segments for classification purposes (R2C), effectively leveraging the continuous signal to predict temporal segments.

The auto-regressive (AR) model excels in short-term predictions with accurate sequential anticipation in the initial minutes. Yet, its performance declines over longer horizons, struggling to maintain coherence and capture phase transitions effectively. This highlights the challenge of preserving consistency in auto-regressive models over extended horizons due to error accumulation.

In the regression task evaluation, we extend the anticipation horizon beyond the previous 5-minute horizon to 15, 30, 45, and 60 minutes, bridging into the remaining surgery duration (RSD) prediction task. Our results show that SWAG-SP achieves the lowest wMAE and inMAE for up to 5-minute horizons, outperforming both the Bayesian model [12] and IIA-Net [13]. While the Bayesian model provides probabilistic reasoning, it lacks short-term precision, and IIA-Net’s reliance on tool-based annotations may limit its feasibility in real-time settings.

Our model also ranks second in the remaining surgery duration benchmark on the Cholec80 dataset. As shown in Table 3, the model performs well against prior approaches, while Fig. 4 illustrates the challenges on the AutoLaparo21 dataset, particularly with certain phases that exhibit variability and abrupt transitions.

Clinically, SWAG offers significant potential. Real-time phase anticipation can alleviate the cognitive load on surgical teams and support intraoperative decision-making by offering foresight into upcoming phases. This predictive support could improve team coordination, potentially reduce surgery times, and enhance patient safety. Furthermore, integrating statistical priors in SWAG-SP\* aligns model outputs with probable workflows, enhancing reliability in clinical applications.

However, precise intraoperative workflow timing prediction faces intrinsic challenges due to anatomical differences, surgeon skill, patient-specific factors, and real-time changes. Surgery is not entirely deterministic, with multiple possible paths leading to optimal outcomes, making accurate long-term prediction especially challenging for generative models. Future work should focus on enhancing the generative process to make the model more reliable and adaptable in clinical scenarios. Integrating language inputs would allow the model to respond directly to prompts or instructions from the surgical team, facilitating a more interactive AI system. Extending SWAG towards a vision-language-action framework would enable the model to process visual and instructional inputs, supporting the prediction of both coarse and fine-grained aspects of the surgical workflow.

## 6 Conclusion

In this work, we introduce SWAG, a novel model unifying surgical phase recognition and long-term generative-based anticipation within a single framework enhanced by successfully embedding prior knowledge in future-generated tokens. Evaluations on the Cholec80 and AutoLaparo21 datasets demonstrate that SWAG outperforms naive baselines in classification and achieves competitive results in regression tasks, specifically for remaining surgery duration predictions. To support its clinical integration, we have demonstrated SWAG’s utility within a software application<sup>1</sup>. This work establishes SWAG as a novel framework in surgical workflow anticipation to support intraoperative guidance.

## Declarations

The authors declare no conflict of interest. This article does not contain any studies with human participants or animals performed by any of the authors. This manuscript does not contain any patient data.

## References

- [1] Sexton, K., Johnson, A., Gotsch, A., Hussein, A.A., Cavuoto, L., Guru, K.A.: Anticipation, teamwork and cognitive load: chasing efficiency during robot-assisted surgery. *BMJ Quality & Safety* (2018)
- [2] Yurko, Y.Y., Scerbo, M.W., Prabhu, A.S., Acker, C.E., Stefanidis, D.: Higher mental workload is associated with poorer laparoscopic performance as measured by the nasa-tlx tool. *Simulation in Healthcare* (2010)
- [3] Czempiel, T., Paschali, M., Keicher, M., Simson, W., Feußner, H., Kim, S.T., Navab, N.: Tecno: Surgical phase recognition with multi-stage temporal convolutional networks. *International Conference on Medical Image Computing and Computer-Assisted Intervention* (2020)
- [4] Liu, Y., Boels, M., García-Peraza-Herrera, L.C., Vercauteren, T.K.M., Dasgupta, P., Granados, A., Ourselin, S.: Lovit: Long video transformer for surgical phase recognition. *Medical Image Analysis* (2023)
- [5] Liu, Y., Huo, J., Peng, J., Sparks, R., Dasgupta, P., Granados, A., Ourselin, S.: Skit: a fast key information video transformer for online surgical phase recognition. In: *Proceedings of the IEEE/CVF International Conference on Computer Vision* (2023)
- [6] Aksamentov, I., Twinanda, A.P., Mutter, D., Marescaux, J., Padoy, N.: Deep neural networks predict remaining surgery duration from cholecystectomy videos. In: *MICCAI 2017* (2017). Springer

---

<sup>1</sup><https://maxboels.github.io/swag>

- [7] Twinanda, A.P., Yengera, G., Mutter, D., Marescaux, J., Padoy, N.: Rsdnet: Learning to predict remaining surgery duration from laparoscopic videos without manual annotations. *IEEE transactions on medical imaging* (2018)
- [8] Rivoir, D., Bodenstedt, S., Bechtolsheim, F., Distler, M., Weitz, J., Speidel, S.: Unsupervised temporal video segmentation as an auxiliary task for predicting the remaining surgery duration. *OR/MLCN@MICCAI* (2019)
- [9] Marafioti, A., Hayoz, M., Gallardo, M., Márquez Neila, P., Wolf, S., Zinkernagel, M., Sznitman, R.: Catanet: predicting remaining cataract surgery duration. In: *MICCAI 2021 Conference, Strasbourg, France* (2021). Springer
- [10] Wu, J., Zou, X., Tao, R., Zheng, G.: Nonlinear regression of remaining surgery duration from videos via bayesian lstm-based deep negative correlation learning. *Computerized Medical Imaging and Graphics* (2023)
- [11] Wijekoon, A., Das, A., Herrera, R.R., Khan, D.Z., Hanrahan, J., Carter, E., Luoma, V., Stoyanov, D., Marcus, H.J., Bano, S.: Pitrsdnet: Predicting intra-operative remaining surgery duration in endoscopic pituitary surgery (2024)
- [12] Rivoir, D., Bodenstedt, S., Funke, I., Bechtolsheim, F., Distler, M., Weitz, J., Speidel, S.: Rethinking anticipation tasks: Uncertainty-aware anticipation of sparse surgical instrument usage for context-aware assistance. *International Conference on Medical Image Computing and Computer-Assisted Intervention* (2020)
- [13] Yuan, K., Holden, M., Gao, S., Lee, W.: Anticipation for surgical workflow through instrument interaction and recognized signals. *Medical Image Analysis* (2022)
- [14] Radford, A., Wu, J., Child, R., Luan, D., Amodei, D., Sutskever, I.: Language models are unsupervised multitask learners. *OpenAI blog* (2019)
- [15] Wang, J., Chen, G., Huang, Y., Wang, L., Lu, T.: Memory-and-anticipation transformer for online action understanding. *ICCV* (2023)
- [16] Blum, T., Feußner, H., Navab, N.: Modeling and segmentation of surgical workflow from laparoscopic video. In: *MICCAI* (2010)
- [17] Twinanda, A.P.: Vision-based approaches for surgical activity recognition using laparoscopic and RBGD videos. PhD thesis, University of Strasbourg (2017)
- [18] Vaswani, A., Shazeer, N., Polosukhin, I.: Attention is all you need. *NIPS* (2017)
- [19] Dosovitskiy, A., Beyer, L., Kolesnikov, A., Weissenborn, D., Zhai, X., Unterthiner, T., Dehghani, M., Minderer, M., Heigold, G., Gelly, S., Uszkoreit, J., Houlsby, N.: An image is worth 16x16 words: Transformers for image recognition at scale. *International Conference on Learning Representations* (2020)

- [20] Gao, X., Jin, Y., Long, Y., Dou, Q., Heng, P.: Trans-svnet: Accurate phase recognition from surgical videos via hybrid embedding aggregation transformer. In: Bruijne, M., Cattin, P.C., Cotin, S., Padoy, N., Speidel, S., Zheng, Y., Essert, C. (eds.) *Medical Image Computing and Computer Assisted Intervention - MICCAI 2021*. Springer, ??? (2021)
- [21] Ginesi, M., Meli, D., Roberti, A., Sansonetto, N., Fiorini, P.: Autonomous task planning and situation awareness in robotic surgery. *IEEE/RJS International Conference on Intelligent RObots and Systems* (2020)
- [22] Qin, Y., Feyzabadi, S., Allan, M., Burdick, J., Azizian, M.: davincinet: Joint prediction of motion and surgical state in robot-assisted surgery. *IEEE/RJS International Conference on Intelligent RObots and Systems* (2020)
- [23] Zhang, J., Zhou, S., Wang, Y., Shi, S., Wan, C., Zhao, H., Cai, X., Ding, H.: Laparoscopic image-based critical action recognition and anticipation with explainable features. *IEEE Journal of Biomedical and Health Informatics* (2023)
- [24] Ban, Y., Rosman, G., Eckhoff, J.A., Ward, T.M., Hashimoto, D.A., Kondo, T., Iwaki, H., Meireles, O.R., Rus, D.: Supr-gan: Surgical prediction gan for event anticipation in laparoscopic and robotic surgery. *IEEE Robotics and Automation Letters* (2022)
- [25] Yin, L., Ban, Y., Eckhoff, J., Meireles, O., Rus, D., Rosman, G.: Hypergraph-transformer (hgt) for interactive event prediction in laparoscopic and robotic surgery (2024)
- [26] Zhang, X., Moubayed, N.A., Shum, H.P.H.: Towards graph representation learning based surgical workflow anticipation. *2022 IEEE-EMBS International Conference on Biomedical and Health Informatics (BHI)*, 01–04 (2022)
- [27] Twinanda, A.P., Shehata, S., Mutter, D., Marescaux, J., Mathelin, M., Padoy, N.: Endonet: A deep architecture for recognition tasks on laparoscopic videos. *IEEE Trans. Medical Imaging* **36**(1), 86–97 (2017)
- [28] Wang, Z., Lu, B., Long, Y., Zhong, F., Cheung, T.-H., Dou, Q., Liu, Y.: Autolaparo: A new dataset of integrated multi-tasks for image-guided surgical automation in laparoscopic hysterectomy. In: *International Conference on Medical Image Computing and Computer-Assisted Intervention*, pp. 486–496 (2022). Springer
- [29] Jin, Y., Long, Y., Gao, X., Stoyanov, D., Dou, Q., Heng, P.-A.: Trans-svnet: hybrid embedding aggregation transformer for surgical workflow analysis. *International Journal of Computer Assisted Radiology and Surgery* (2022)

## 7 Supplementary Material

### 7.1 Implementation Details

Our experiments were conducted on a single NVIDIA Tesla V100 GPU. We used a 12-head, 12-layer Transformer encoder as our spatial feature extractor, based on the ViT-B/16 architecture following LoViT [4]. This model was pre-trained on ImageNet 1K (IN1k) and produced 768-d representations, with an input image size of  $248 \times 248$  pixels. For training the spatial feature extractor, we used stochastic gradient descent with momentum for 35 epochs, with a 5-epoch warm-up period and a 30-epoch cosine annealed decay. We used a batch size of 16 and a learning rate of 0.1, which was multiplied by 0.1 at the 20th and 30th epochs. We set the weight decay to  $1e-4$  and the momentum to 0.9. For the past-present encoder, we used an input clip length  $l$  of 1440 frames or 24 minutes at 1fps with a sliding context length window  $w$  of 20 frames, generating 512-d feature vectors. Key-pooled feature dimensions  $d$  are 64-d and 32-d on Cholec80 and AutoLaparo21, respectively. The temporal modules underwent training for 40 epochs using SGD and momentum with a learning rate of  $3e-4$ , weight decay of  $1e-5$ , a 5 epoch warm-up period, and a 35 epoch cosine annealed decay, with a batch size of 8.

### 7.2 Future Tokens Embedding Initialization

This process involves generating a final input embedding  $\mathbf{x}_\tau$  for each future token  $\tau$  by combining the initial embedding  $\mathbf{e}_\tau$ , the probability vector  $\mathbf{p}_\tau$  projected into a higher-dimensional space, and positional encoding, ultimately forming the input for the transformer decoder.

$$\mathbf{p}_\tau = \mathbf{P}_{i::,\tau} \quad \text{for } \tau = 1, 2, \dots, 15 \quad (2)$$

$$\mathbf{h}_\tau = W_p \mathbf{p}_\tau + \mathbf{b}_p \quad (3)$$

$$\mathbf{x}_\tau = \text{LayerNorm}(\mathbf{e}_\tau + \alpha \mathbf{h}_\tau + \text{PositionalEncoding}(\tau)) \quad (4)$$

### 7.3 Ablation Studies

We conducted ablation experiments to study the impact of various factors on model performance, including context length, anticipation interval, number of context tokens, temporal pooling methods, and model size.

**Context Length.** Figure 5 (Supplementary Material) shows that a context length of 24 minutes yields the highest mean cumulative accuracy on both datasets.

**Compression and Anticipation Time.** Figure 6 indicates that a 1-minute interval between input samples produces the highest accuracies on both datasets.

**Temporal Pooling Methods.** Figure 7 compares global and interval pooling methods. Single-pass decoding with global context tokens consistently outperforms auto-regressive decoding with either temporal pooling methods for all numbers of context tokens and on both datasets.

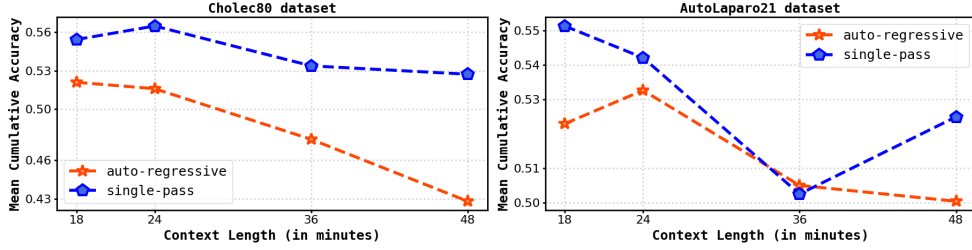


Fig. 5: Context Length (in minutes) of the input sequence.

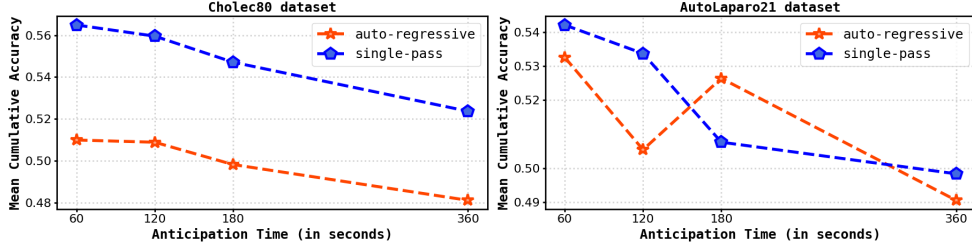


Fig. 6: Effect of the anticipation time between frames during training (in seconds) on the test accuracy.

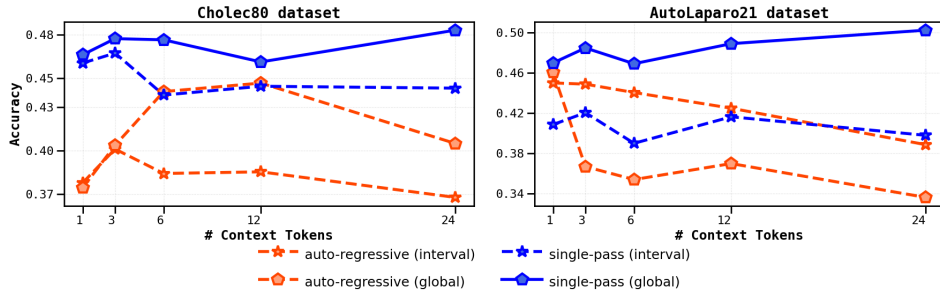


Fig. 7: Number of context tokens with a fixed context length of 24 minutes i.e. compression of input sequence with global and interval temporal pooling methods.

**Model Size.** Figure 8 demonstrates that medium-sized models achieve the best overall accuracies, with the optimal model size varying slightly between datasets. These ablations indicate that careful tuning of these parameters can significantly impact long-term surgical phase anticipation performance.

**Standard Deviation.** To assess the stability and robustness of the models, we depict the standard deviation of the anticipation accuracies across different videos. As shown



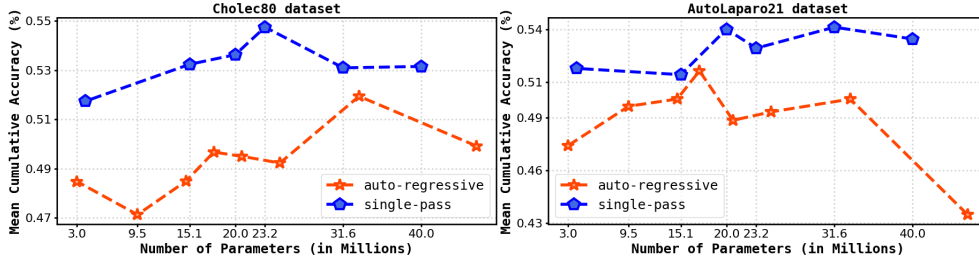


Fig. 8: Model size (million parameters) over accuracy.

in Fig.9, the single-pass method has a lower variance on Cholec80 and, conversely, a higher variance on AutoLaparo21.

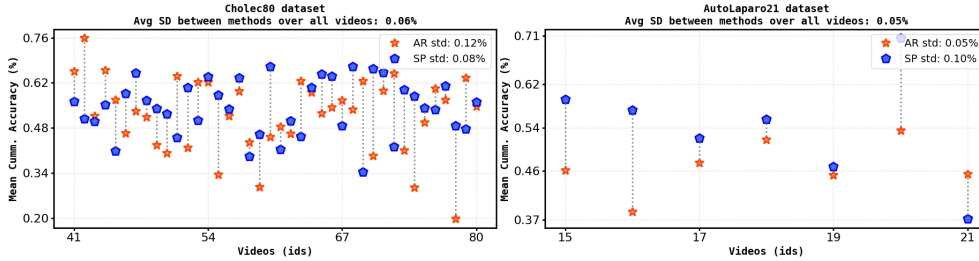
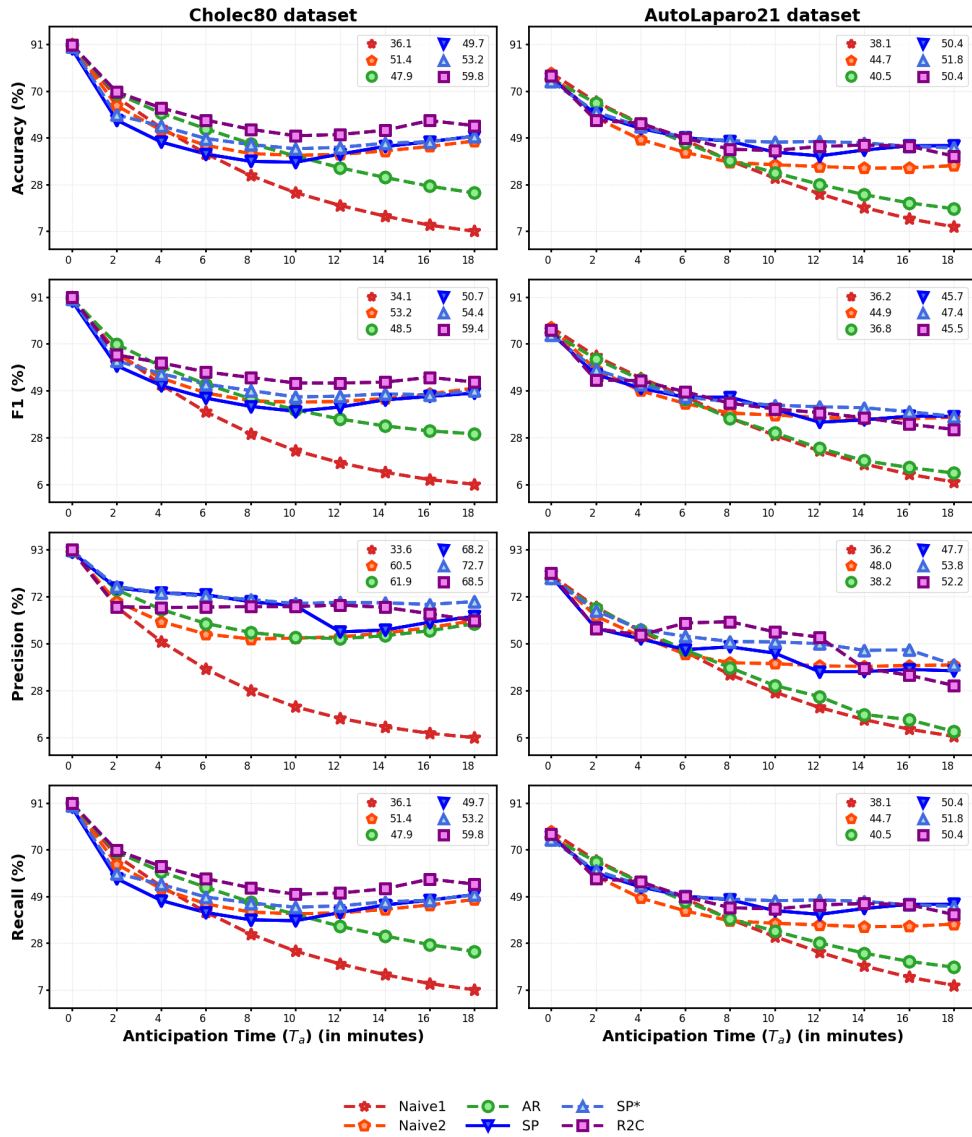


Fig. 9: Standard Deviation between videos accuracy.

**Other Ablations.** Additionally, we explored multiple dimensions and layers for both the recognition and prediction modules in Table 4. Finally, we include the F1, Precision, and Recall evaluation metrics in Fig. 10, although we argue that the class distribution is well-balanced as our testing videos correspond to real surgeries.

Table 4: Model size and Architecture used in this study.

Size	#Param	Rec-Encoder			Pred-Decoder	
		Dim	Layer/Head	Dec	Dim	Layer/Head
L	46M	512	2/8	✓	512	10/8
M	24M	512	2/8	✓	384	6/8
S	17M	512	2/8	✓	256	4/8
XS	9M	384	2/8	✓	128	2/4
XXS	3M	256	2/8		128	2/4



**Fig. 10:** Evaluation metrics for each method on both datasets: Accuracy, F1, Precision, and Recall.